JOURNAL OF APPLIED ELECTROCHEMISTRY 1 (1971) 103–112

Fluidized bed electrodes Part IV. Electrodeposition of copper in a fluidized bed of copper-coated spheres

M. FLEISCHMANN, J. W. OLDFIELD* and L. TENNAKOON

Department of Chemistry, The University, Southampton, U.K.

Received 2 January 1971

The effective resistivity of the discontinuous metal phase in a fluidized bed copper electrode is derived from measurements of the potential distribution in the solution. The values are similar to those which have been previously observed for a fluidized bed of silver-coated particles and are compared with a theoretical expression based on a model of charge sharing during single particle elastic collisions. It is shown that the metal resistivity follows the predicted dependence on bed expansion and solution resistivity; the constant of proportionality is, however, different and this is attributed to a stagnation zone close to the feeder electrode. Such a stagnant zone is also indicated by comparison of the experimental and theoretically predicted distribution of potential in the metal phase.

The diffusion controlled removal of copper from 10^{-4} M copper sulphate is also shown to follow the theoretically predicted behaviour; the mass transfer coefficient indicates a high degree of turbulence within the bed. It is shown that scale-up factors of the order of 300 can be achieved in the processing of such dilute solutions. In view of the relatively high resistivity of the metal phase it is suggested that practical systems would arrange for a current and fluid flow to be at right angles to each other.

It has been shown recently that fluidized beds of conducting particles in a stream of electrolyte behave as three-dimensional electrodes [1] which are suitable for the design of a number of electrochemical reactors. Data have been published for a variety of systems [2–7] which include the deposition of metal from dilute solutions [3] (zinc from alkaline zincate) and the rapid dissolution of the metal in a metal/air cell. For certain of these applications the high rate of mass transfer to the surface of the particles and the large surface area per unit volume of the fluidized beds are of particular advantage; for example, it is possible to deposit zinc at a high rate without the formation of dendrites.

In a recent theoretical approach to electrodes of this kind [8] polarization equations and potential profiles within fluidized beds were derived by assigning an effective resistivity, ρ_m, to the discontinuous metal phase. The three-dimensional electrode was treated in the usual manner by using a one-dimensional model [9, 10], the variation of the current density, potential etc. only being considered as a function of the 'depth' of the electrode. In this treatment the model was simplified by assuming both ρ_m and the effective resistivity of the solution, ρ_s, to be constant throughout the bed, i.e. any variation of ρ_s with voidage and of ρ_m with varying turbulence near the point of entry, were neglected. The cases of activation control close to and far from the equilibrium potential, as well as of diffusion control to the surface of the particles were discussed.

In a further paper [11] an *a priori* expression for ρ_m was derived based on the assumption of

* Present address: International Nickel Ltd., Research Laboratories, Wiggin Street, Birmingham, 16.

charge sharing between the particles following elastic collisions in the fluidized bed. These theories have been tested by studying the reduction of oxygen in alkaline solutions in a fluidized bed of silver-coated glass spheres [12] where the theory relating to diffusion controlled and activation controlled reactions [8] was verified. Values of ρ_m determined from the Tafel plots of the polarization curves gave qualitative agreement with the model which has been proposed for this parameter [11] but no attempt was made to test the predicted variation of ρ_m with the experimental parameters.

It is clear that the value of the resistivity of the metal phase, which is a characteristic parameter of such fluidized beds, will determine the design of the electrode structures. The aim of the work reported in this paper has therefore been to investigate continuous metal deposition from dilute solutions in fluidized electrodes and to test the theoretical expression which has been derived for ρ_m, namely,

$$\rho_m = \frac{0{\cdot}28\ \varepsilon^{\frac{3}{2}}\ (\varepsilon^{\frac{1}{2}}-1)\gamma^{\frac{1}{2}}\ \rho_s}{\rho^{\frac{1}{2}}\ v_\rho^{\frac{3}{2}}} \qquad (1)$$

where ε is the electrode length normalized with respect to the static electrode, γ is Young's modulus, ρ is the density difference between the solid and liquid and v_p is the mean particle velocity. The system chosen was the electrodeposition of copper from acid solutions of cupric ions

$$Cu^{2+} + 2e \rightleftharpoons Cu. \qquad (2)$$

This reaction has been studied in detail by other authors [13, 14] and their kinetic data have been used throughout this work.

Experimental

Instrumentation

All experiments were carried out potentiostatically using a Chemical Electronics potentiostat (model 20/20A). A Chemical Electronics linear sweep generator in conjunction with the potentiostat was used to obtain current-voltage curves. All recordings were made on a Rikadenki Kogyo *Y-t* recorder (model B14).

Solution Preparation

Solutions 10^{-2}M and 10^{-4}M in $CuSO_4$ in a supporting electrolyte of 1M H_2SO_4 were used in all the experiments. The solutions were made up from AnalaR reagents and triply distilled water. All experiments were carried out in deoxygenated solutions under nitrogen gas. In the case of the more dilute copper sulphate solution remaining traces of oxygen were first removed by prior electrolysis on the fluidized copper electrode and the appropriate amount of copper sulphate was then added to the circulating system via a serum cap by using a hypodermic syringe.

Solutions were analysed spectrophotometrically for copper [15] with 'Fast sulphon Black F' reagent at pH 11. An SP 800 spectrophotometer was used and extinction coefficients were measured at 630 mμ.

Fluidized electrode material

Solid copper particles and copper coated ballotini glass spheres in the size range 450–520 μ diameter were used as the fluidized bed material. The copper was deposited onto the glass by an electroless method described elsewhere [16].

The area per cc of the fluidized bed, A, was calculated using the formula,

$$A = 3(1-V)/r \qquad (3)$$

where r was taken as the mean sieve size used in separating the particles and where the voidage is given by

$$V = (1-(V-V_o)/\varepsilon). \qquad (4)$$

The voidage of a packed bed, V_o, was determined by measurement of the volume of liquid displaced by a given volume of spheres.

Throughout this work it was essential that the effective area per unit volume of a fluidized bed of copper coated particles should be reproducible. It is known [17] however, that if copper is deposited from solution onto a copper substrate under conditions of diffusion control, the surface roughness of the deposit can increase rapidly and that under these conditions A would therefore increase. The criterion used for the constancy of A was the reproducibility of the polarization curves and this was achieved by the

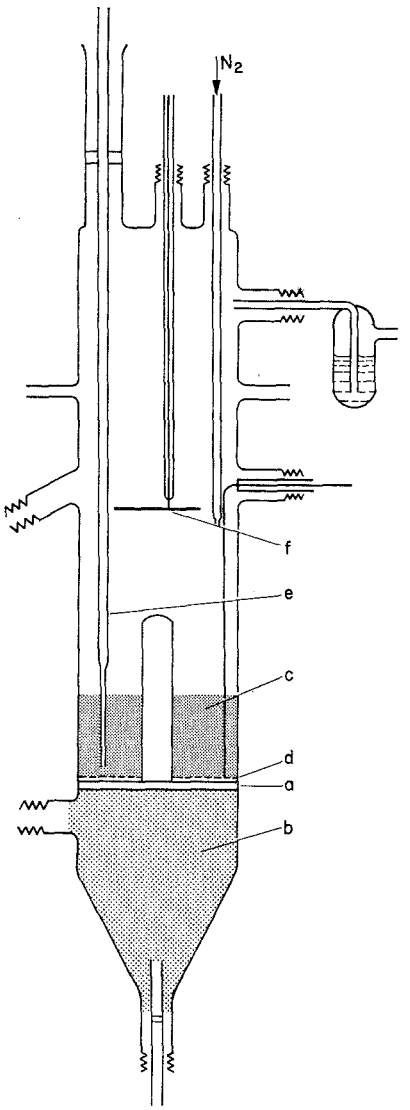

Fig. 1. Schematic diagram of electrochemical cell used.

following procedure. Prior to recording a polarization curve the fluidized bed electrode was held at an anodic potential such that an anodic current of the order of 0·1 mA cm^{-2} passed for 5 to 10 s.

Electrochemical cells

The electrochemical cell used for the measurement of polarization curves and potential profiles is shown schematically in Fig. 1. A grade 0 sintered glass disc *a*) of diameter 3·6 cm was used both as the bed support and flow distributor. A glass cylinder of diameter 1 cm and height 3·5 cm, closed flat at either end, was centrally sealed onto the sinter to facilitate an even flow distribution. A bed of glass spheres *b*) was packed below the sinter, as it was observed in preliminary experiments that this improved the fluidization of the copper coated beads used as the working electrode *c*).

A mesh copper gauze *d*), positioned on top of the sinter, was used as the feeder electrode, contact being made via a copper wire insulated with Lacomit lacquer. One of two reference electrodes was used, either a copper wire or a $Hg/HgSO_4/1M\ H_2SO_4$ electrode. In obtaining polarization curves, the Luggin capillary *e*) was positioned close to the feeder electrode via the top of the cell, whereas in determining potential profiles the reference electrode was placed below the sinter. The counter electrode was a flat spiral of copper wire *f*).

The solution was pumped through the cell by means of a Charles Austin C.25 centrifugal pump with the impeller and pump made of polypropylene and the shaft made of titanium. The flow rate was monitored on a Gap flowmeter fitted with p.t.f.e. nozzle inserts and a cored plastic float.

Two probe electrodes were used to determine the potential profiles. In order to measure the variation of potential in the solution a glass tube probe with an external diameter of 0·15 cm was used, the internal diameter being small enough to prevent the entry of the particles. The upper end of the probe terminated in a socket into which an $Hg/Hg_2SO_4/1MH_2SO_4$ reference electrode was fitted. The potential profile in the metal was measured with a copper sphere of diameter 0·1 cm attached to the end of a copper wire sealed into a 0·4 cm diameter glass tube. The exposed portion of the wire was insulated with Lacomit lacquer. The probes were moved vertically through the solution at a rate of 0·85 cm min^{-1} by using a synchronous motor driving a screw reduction gear.

A cell somewhat similar to that shown in Fig. 1 was used for measurements on the removal of copper from $10^{-4}M\ CuSO_4$ solution under diffusion controlled conditions. In this cell a platinum counter electrode was used and this was separated from the electrolyte stream by an ion

exchange membrane so as to minimize concentration changes in the catholyte; the central cylinder shown in Fig. 1 was also omitted.

Results and interpretation

In the theoretical treatment of fluidized bed electrodes [8] it has been assumed that the Volmer expression

$$i = i_o\left\{\exp\frac{(\alpha nF\eta)}{RT} - \exp\frac{(\alpha-1)nF\eta)}{RT}\right\} \qquad (5)$$

is valid. However, because of the relative complexity of this expression it was only possible to derive the polarization equations and the metal and solution potential profiles within the electrode for two limiting cases, firstly when $\eta \gg RT/\alpha nF$ and therefore, for a cathodic reaction

$$i = i_o \exp\frac{((\alpha-1)nF\eta)}{RT} \qquad (6)$$

and secondly when $\eta \ll RT/\alpha nF$ and therefore

$$i = \frac{i_o nF\eta}{RT}. \qquad (7)$$

Thus values of the effective metal resistivity, ρ_m, can be determined by comparing experimental results with theoretical predictions at either low or high overpotentials; the experimental results can be in the form of polarization curves, or solution or metal potential profiles in the direction of current flow. Furthermore, it is possible to place the feeder electrode at the top of the bed, i.e. on the side nearest to the counter electrode, Fig. 1. Results have been obtained for both configurations under all these conditions [18]. Fig. 2 shows a typical set of such polarization curves obtained at different fluidized bed expansions for the electrodeposition of copper using the configuration shown in Fig. 1 and using 10^{-2}M $CuSO_4$ solution.

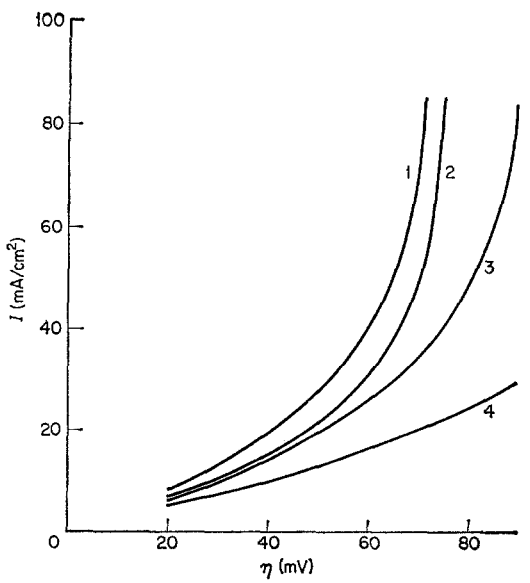

Fig. 2. Polarization curves at various electrode expansions; 1:13%; 2:18%; 3:22%, 4:27%.

For the deposition of copper it is assumed that $\alpha = 0{\cdot}5$ [13, 14] and therefore $RT/\alpha nF = 25{\cdot}7$ mV; thus to determine values of ρ_m from these polarization curves it is necessary that, for Equation (6) to hold to within 2% $\eta \geqslant 50$ mV and for Equation (7) to hold to within 2·5% $\eta \leqslant 5$ mV. Because of the overall accuracy of the experimental technique, results in the range 0–5 mV overpotential can at best only be used to give an approximate estimate of the value of ρ_m. At high overpotentials the evolution of hydrogen occurs, thus imposing a limit on the range over which Equation (6) is applicable. In view of this it was decided to determine values of ρ_m from potential profiles at a value of η such that Equation (6) is applicable throughout the electrode and that no hydrogen evolution occurred in any part of the bed. The value of the overpotential at the feeder electrode, ϕ_m^o, was therefore chosen to be 50 mV. Under these conditions, Fig. 3, the maximum potential drop through the solution within the electrode, in the direction of current flow, was of the order of 100 mV, and therefore, as the reversible potential for copper deposition under the conditions used is 288 mV *v.* NHE no hydrogen evolution could occur.

The theoretical expression for the solution potential profile under conditions of high overpotential, has been shown to be

$$\cos^{-1}\left\{1-\frac{I^2\rho_m^2}{\beta(\rho_m+\rho_s)}\exp f\phi_m^o\right\}^{\frac{1}{2}}$$

$$-\cos^{-1}\left\{\frac{1-\dfrac{I^2\rho_m^2}{\beta(\rho_m+\rho_s)}\exp f\phi_m^0}{\exp f(I\rho_m x+(1+\rho_m/\rho_s)\phi_s)}\right\}^{\frac{1}{2}}$$

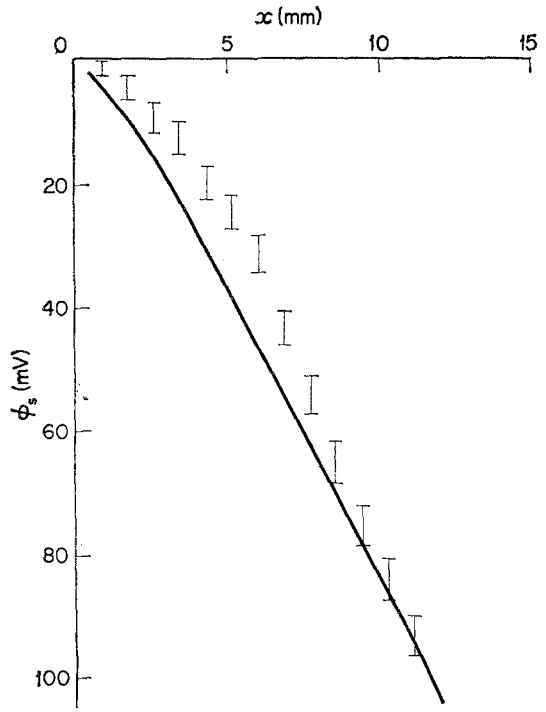

Fig. 3. Comparison of theoretical (—) and experimental (I) solution potential profiles:

a) 13·6% expansion, $A = 57{\cdot}2\ \text{cm}^{-1}$, $i_o = 0{\cdot}96\times10^{-3}$ A cm^{-2}, $\rho_m = 39{\cdot}8\ \Omega$ cm, $\rho_s = 4{\cdot}67\ \Omega$ cm, $\phi_m^0 = -50{\cdot}1\times10^{-3}$V, $I = 23{\cdot}6\times10^{-3}$ A cm^{-2}.

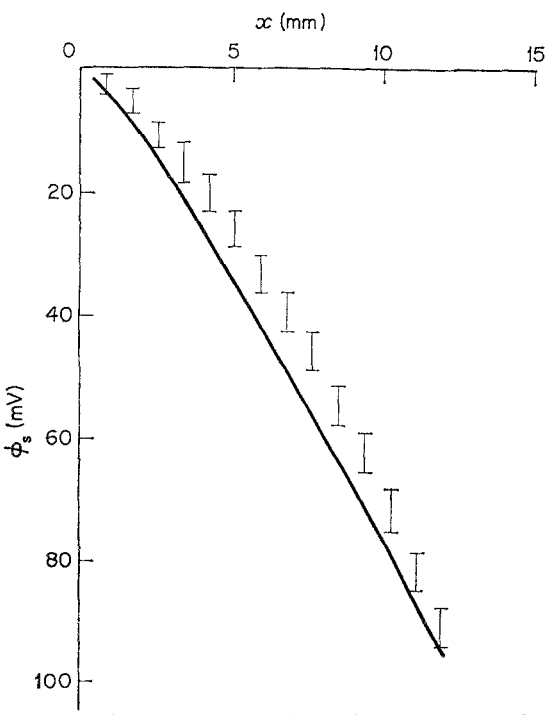

b) 18·2% expansion, $A = 55\ \text{cm}^{-1}$, $i_o = 0{\cdot}96\times10^{-3}$ A cm^{-2}, $\rho_m = 49{\cdot}5\ \Omega$ cm $\rho_s = 4{\cdot}52\ \Omega$ cm, $\phi_m^0 = -51{\cdot}4\times10^{-3}$ V, $I = -21\times10^{-3}$ A cm^{-2}.

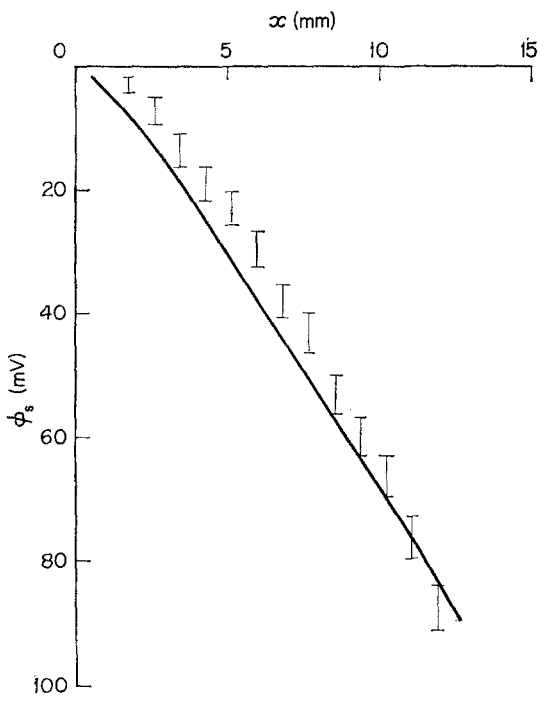

c) 22·7% expansion, A = 53 cm^{-1}, $i_o = 0{\cdot}96\times10^{-3}$ A cm^{-2}, $\rho_m = 56{\cdot}1\ \Omega$ cm, $\rho_s = 4{\cdot}4\ \Omega$ cm, $\phi_m^0 = -51{\cdot}9\times10^{-3}$ V, $I = -19{\cdot}5\times10^{-3}$ A cm^{-2}.

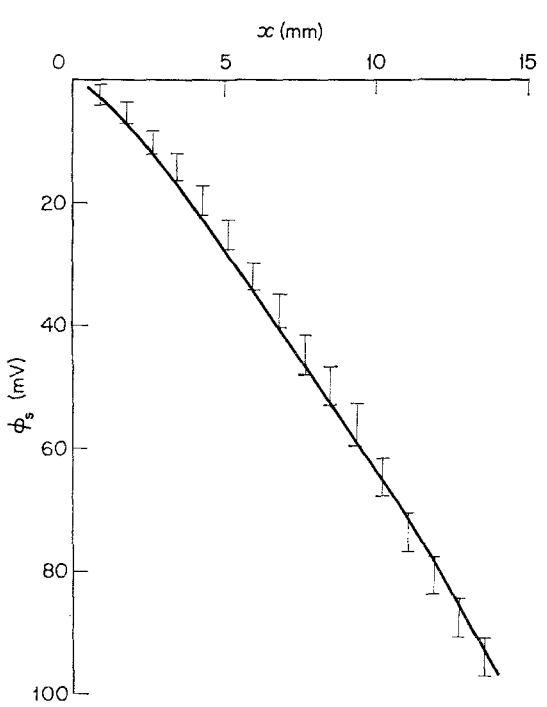

d) 27% expansion, $A = 51\ \text{cm}^{-1}$, $i_o = 0{\cdot}96\times10^{-3}$ A cm^{-2}, $\rho_m = 61{\cdot}15\ \Omega$ cm $\rho_s = 4{\cdot}26\ \Omega$ cm, $\phi_m^0 = -51{\cdot}4\times10^{-3}$ V, $I = 18\times10^{-3}$ A cm^{-2}.

$$= \frac{xf\beta^{\frac{1}{2}}(\rho_m+\rho_s)^{\frac{1}{2}}}{2}\left\{1-\frac{I^2\rho_m^2}{\beta(\rho_m+\rho_s)}\exp f\phi_m^0\right\}^{\frac{1}{2}} \times \exp\frac{f\phi_m^0}{2} \quad (8)$$

where

$$\beta = \frac{2i_oART}{(1-\alpha)nF} \quad (9)$$

and

$$f = \frac{(1-\alpha)nF}{RT}. \quad (10)$$

This is related to the potential in the metal phase by the relationship

$$\phi_m = \phi_m^0 - I\rho_m x - \phi_s\rho_m/\rho_s. \quad (11)$$

Equations (8) to (11) are written for a cathodic reaction, the potentials and currents containing their sign, i.e. ϕ_m^0 and ϕ_m are negative, ϕ_s is positive and I is negative.

Values of ρ_m were therefore obtained by fitting Equation (8) to the experimentally determined solution potential profiles by variation of this single parameter. The theoretical metal potential profiles were then calculated using Equation (11) and compared to experiment to check the consistency of the theory.

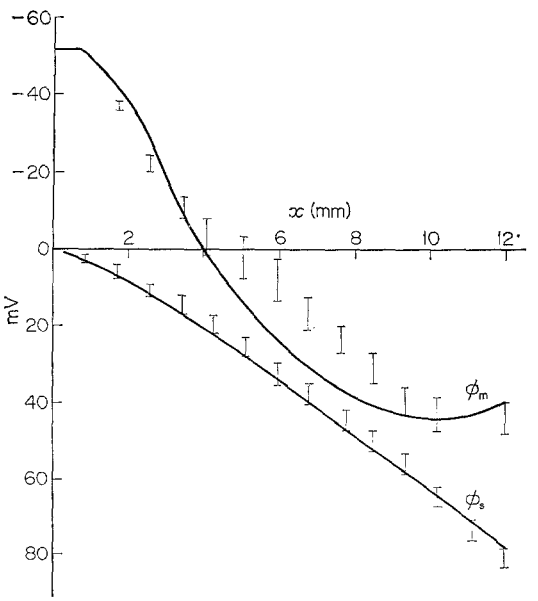

Fig. 4. Comparison of theoretical (—) and experimental metal and solution (I) potential profiles for the following set of parameters: $A = 51$ cm^{-1}, $i = 0{\cdot}96\times10^{-3}$ A cm^{-2}, $\rho_m = 65{\cdot}2$ Ω cm $\rho_s = 4{\cdot}26$ Ω cm, $\phi_m^0 = -51{\cdot}4\times18^{-3}$ V, $I = -17{\cdot}4\times10^{-3}$ A cm^{-2}, $x_o = 0{\cdot}071$ cm.

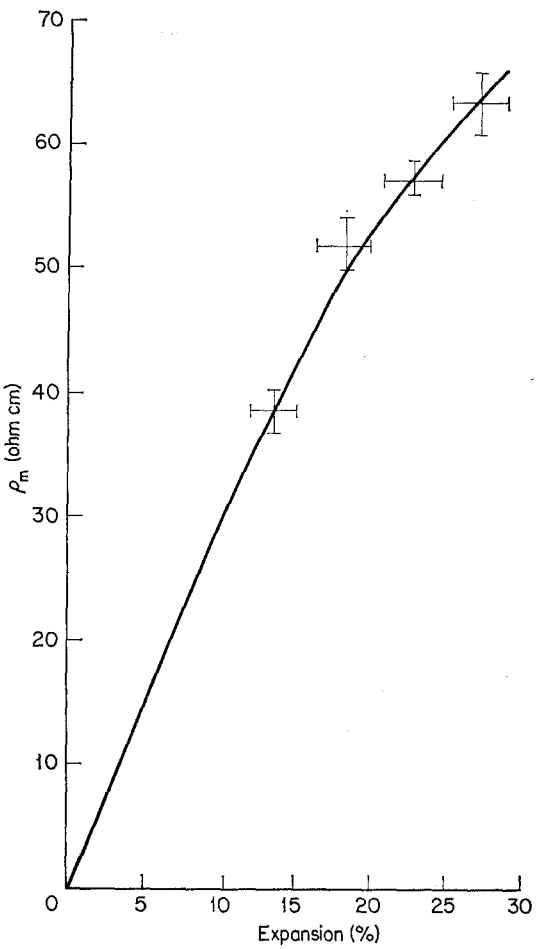

Fig. 5. Metal resistivity as a function of expansion.

Fig. 3*a–d* shows a series of experimental and theoretical potential profiles in the solution for different electrode expansions. Good agreement is obtained between theory and experiment at high expansions, Fig. 3*d*, but as the expansion decreases the deviation between the two increases slightly indicating that some of the assumptions made in [8] are beginning to break down. The consistency of the theory is checked in Fig. 4 where both the metal and solution potential profiles are compared with the theory, the former being calculated using Equation (11). In order to obtain the agreement shown in Fig. 6 for the potential profile in the metal phase, it was necessary to use $(x-0{\cdot}071)$ instead of x in Equation (11), indicating that there was a certain

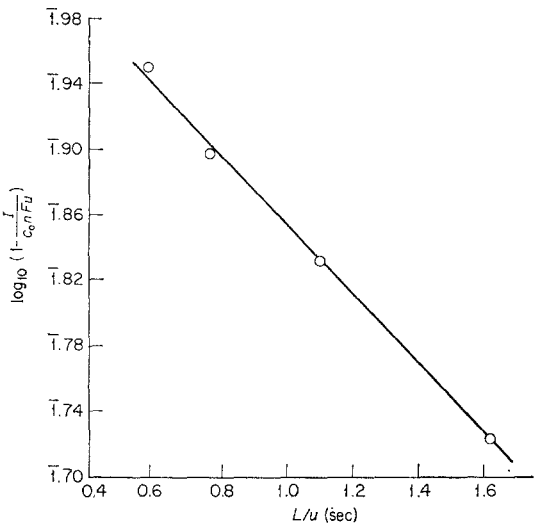

Fig. 6. Variation of current with L/u according to Equation (14) for diffusion controlled deposition. Solid copper particles, 420 μ–500 μ diameter; $u = 2{\cdot}8$ cm s^{-1}.

amount of stagnation close to the feeder electrode (see discussion). This shift in the origin causes the minimum in the calculated profile for the metal phase at bed depths of about 1 cm, whereas the boundary conditions [8] demand that ϕ_m should approach its final value asymptotically. It should also be noted that the local potential difference within the electrode, illustrated in Fig. 4, drops to approximately 30 mV and that under these conditions Equation (6) is only accurate to within 10%, the predicted current therefore being larger than the experimental value; this would result in the predicted drop in the solution potential within the bed being larger than the experimental value and this is, in fact, the direction of the deviations that occur. However, in general the deviation between theory and experiment is small enough that the values of ρ_m obtained can be considered meaningful, and these are shown in Fig. 5 as a function of the percentage electrode expansion.

It was found that the electrodeposition of copper from 10^{-4}M $CuSO_4$ onto the solid copper powder could be carried out at about 99% coulombic efficiency as determined from the comparison of the charge passed with the concentration change in solution. It was found that with increasing negative potential the current reached a well-defined limiting value which varied with the flow rate. At this point the deposition is diffusion controlled throughout the bed and it has been shown [8] that the limiting current is given by

$$I = c_0 nfu\left[1-\exp-\frac{L}{\lambda}\right] \qquad (12)$$

where c_0 is the concentration at the point of entry, L is the bed length and the characteristic length λ is given by

$$\lambda = \frac{\delta u}{DAV} \qquad (13)$$

where D is the diffusion coefficient. The thickness δ of the diffusion layer has a formal significance only since the solution flow is turbulent. Fig. 6 shows a plot of the data according to the equation

$$\log\left[1-\frac{I}{c_0 nFu}\right] = -\frac{DAVL}{2{\cdot}303\,\delta u}. \qquad (14)$$

Discussion

The results obtained allow the validity of the theory relating to the parameter ρ_m to be tested [11]. The complete expression derived for ρ_m when considering systems of practical interest, i.e. $50<r<500$ μ, $1\leqslant\varepsilon\leqslant 1{\cdot}25$ and $v_p\leqslant 40$ cm s^{-1}, is

$$\frac{1}{\rho_m} = \frac{2{\cdot}24\,C\,v_p}{\varepsilon^{\frac{1}{3}}(\varepsilon^{\frac{1}{3}}-1)}\left\{1-\exp-\left\{\frac{4\rho}{v_p\gamma\,\rho_s^3 C^3}\right\}^{\frac{1}{3}}\right\}. \qquad (15)$$

Assuming elastic collisions between particles, it was shown that the extent of charge sharing during collision would be small and that Equation (15) could then be simplified by expanding the exponential, neglecting all but the first two terms, giving

$$\rho_m = \frac{0{\cdot}28\,\varepsilon^{\frac{1}{3}}(\varepsilon^{\frac{1}{3}}-1)\gamma^{\frac{1}{3}}\rho_s}{\rho^{\frac{1}{3}}\,v_p^{\frac{2}{3}}}. \qquad (1)$$

Fig. 7 shows the variation of ρ_m with the combined variable $\varepsilon^{\frac{1}{3}}(\varepsilon^{\frac{1}{3}}-1)\rho_s$. The variation is linear within the limits of experimental error, and the intercept is effectively zero as one would expect. This variation implies that v_p is independent of the solution velocity, u, over the range of u studied.

The theoretically predicted variation of ρ_m is also shown in Fig. 7 where it has been assumed that the value of Young's modulus is 10^{12} dynes cm^{-2} (the value for glass is 5·1 to $7{\cdot}1 \times 10^{11}$ dynes cm^{-2} and the value for copper is $12{\cdot}98 \times 10^{11}$ dynes cm^{-2}), $\rho = 2$ g cm^{-3} and $v_p \simeq 2{\cdot}5$ cm s^{-1}. The value of v_p was estimated from the solution interstitial velocity [11], u/V, which varied from 2·28 to 2·87 cms^{-1} over the range of u studied. It is clearly seen that the predicted variation is much more rapid than that determined experimentally, the slopes being 1210 and 180 respectively.

It is worth noting at this stage that the values of ρ_m obtained here are of the same order, but slightly higher than, the values obtained for an electrode of 500 μ diameter silver coated glass spheres [12] for the same electrode configuration. However, with the feeder electrode positioned at the top of the electrode values of ρ_m were obtained [12] which were in much closer agreement with the theoretical expression, Equation (1). This discrepancy was attributed to an 'entrance effect' caused by uneven fluidization close to the feeder electrode when this is positioned on top of the distributor, resulting in variation in expansion throughout the electrode and a certain amount of stagnation close to the feeder.

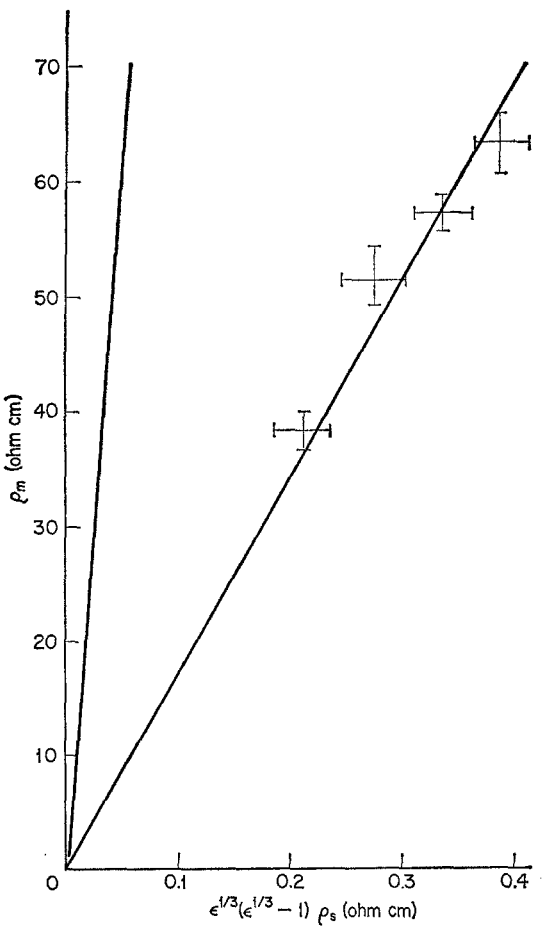

Fig. 7. Metal resistivity as a function of the combined parameter.

From the results of this work we can say that the 'entrance effect' manifests itself in this system by effectively reducing the measured quantity, $\varepsilon^{\frac{1}{3}}(\varepsilon^{\frac{1}{3}}-1)$ by a factor of 6·7. Physically it seems likely that this results from stagnation close to the feeder, and in fact it was necessary to assume a stagnant zone 0·071 cm deep in order to obtain the consistent results shown in Fig. 4 for an electrode operating at an expansion of 27%. As the reaction occurs preferentially close to the feeder electrode (again see Fig. 4) this effect will be a major factor in accounting for the discrepancy.

If the assumptions made in deriving Equation (15) are essentially correct, and the variation of ρ_m with ε and ρ_s is according to Equation (1), then the experimentally obtained values of ρ_m determined for an electrode of silver coated spheres should be 0·9 times the value obtained in this work, the difference arising from the different values of Young's modulus; in fact they are significantly lower. In that investigation, however, the feeder electrode was a flat spiral of nickel wire of diameter 0·15 cm and this did not give such even fluidization as the copper gauze electrode used in the present work; the difference in the values of ρ_m must be attributed to this difference in fluidization.

The results for electrodeposition from 10^{-4}M $CuSO_4$, Fig. 6, show that they fit the model for a diffusion controlled process [8]. From the gradient of the plot values of the mass transfer coefficient $K_m = D/\delta$ of about $1{\cdot}4 \times 10^{-2}$ cm s^{-1} are deduced, indicating a high degree of turbulence within the bed. This high turbulence naturally leads to an efficient depletion of the solution and, for beds 4 cm deep, cross-sectional current densities of 30 mA cm^{-2} could be reached. At a

planar electrode the diffusion controlled current would be $\sim 0{\cdot}1$ mA cm^{-2} under comparable conditions. The results therefore show that scaling up factors of the order of 300 can readily be achieved in the processing of dilute solutions by using fluidized beds as electrodes.

The characteristic length λ derived from Fig. 6 is ~ 6 cm and, allowing for the higher solution velocities used in these measurements, is in line with the characteristic lengths measured for the reduction of oxygen in alkaline solution [12]. It follows that beds containing metal particles and having a depth of less than 30 cm could be used to reduce the concentration of even such dilute solutions by more than two orders of magnitude. In view of the relatively high resistivity of the metal phase the current and fluid flow would be arranged to be at right angles in any practical system and the width of the bed would be of the order of 1 cm. The dimension in the third direction would not, however, be restricted.

Conclusions

From the present investigation we can conclude that for 500 μ diameter particles the variation of ρ_m with ε, and ρ_s is as predicted by Equation (1) and that v_p is independent of the solution velocity u, over the range of u studied, namely 1·22 to 1·68 cm s^{-1}. However, the calculated value of the constant term in Equation (1) i.e. $0{\cdot}28\ \gamma^{\frac{1}{3}}/\rho^{\frac{1}{3}}$ is larger by a factor of 6·7 than the experimentally determined value. This is attributed to the fluidization being non-uniform throughout the bed, the expansion being less at the distributor than at the top of the bed, so much so in fact that a certain amount of stagnation occurs close to the feeder and the term $\varepsilon^{\frac{1}{3}}(\varepsilon^{\frac{1}{3}}-1)$ (which when $(\varepsilon-1)$ is small is proportional to the percentage expansion), is approximately 1/6·7 of the experimentally determined value.

It is possible to achieve diffusion-controlled deposition throughout the fluid bed electrode and the limiting currents follow the predicted equation [8]. The results indicate considerable turbulence within the bed and under these conditions the electrodes can be used to efficiently process dilute solutions.

References

[1] British Patent 1,194,181.
[2] *New Scientist*, **37** (1968) 303.
[3] F. R. Backhurst, F. Goodridge, R. E. Plimley, and M. Fleischmann, *Nature*, **221** (1969) 55.
[4] J. N. Hiddleston and A. F. Douglas, *Nature*, **218** (1968) 601.
[5] R. D. Armstrong, O. R. Brown, R. D. Giles, and J. A. Harrison, *Nature*, **219** (1968) 94.
[6] T. Berent, I. Fells and R. Mason, *Nature*, **223** (1969) 1054.
[7] J. R. Backhurst, J. M. Coulson, M. Fleischmann, F. Goodridge, and R. E. Plimley, *J. Electrochem. Soc.*, **116** (1969) 1600.
[8] M. Fleischmann and J. W. Oldfield, *J. Electroanal. Chem.*, in press.
[9] J. S. Newman and C. W. Tobias, *J. Electrochem. Soc.*, **109** (1962) 1183.
[10] E. A. Grenns II and C. W. Tobias, *Electrochimica Acta*, **10** (1968) 761.
[11] M. Fleischmann and J. W. Oldfield, *J. Electroanal. Chem.*, in press.
[12] M. Fleischmann, J. W. Oldfield, and D. F. Porter, *J. Electroanal. Chem.*, in press.
[13] O. R. Brown and H. R. Thirsk, *Electrochimica Acta*, **10** (1965) 383.
[14] E. Mattson and J. O'M Bockris, *Trans Farad. Soc.*, **55** (1959) 1586.
[15] R. Belcher and A. M. Cabrera, *Anales. Real. Soc. Espan. Fisquim*, **54**(*B*) (1963) 281.
[16] V. I. Shorokhova and L. I. Kuzmin, *Int. Chem. Eng.*, **4** (1969) 451.
[17] N. Ibl and K. Schadegg, *J. Electrochem. Soc.*, **114** (1967) 54.
[18] L. Tennakoon, unpublished data.

Glossary

A surface area per unit volume of electrode (cm^{-1})
C double layer capacity (Farads cm^{-2})
c_o concentration (moles cm^{-3})
D diffusion coefficient (cm^2 s^{-1})
F the Faraday (coulombs mole^{-1})
I total current (A cm^{-2})
i local current density (A cm^{-2})
i_o exchange current density (A cm^{-2})
K_m mass transfer coefficient (cm s^{-1})
n equivalents per mole
R gas constant (volt coulomb deg^{-1} mole^{-1})
r particle radius (cm)
T absolute temperature
u superficial solution velocity (cm s^{-1})
V voidage

v_p mean particle velocity (cm s^{-1})
x distance from feeder in direction of current flow (cm)
α electrochemical transfer coefficient for an anodic reaction
γ Young's modulus (dynes cm^{-2})
δ Solution-metal diffusion layer thickness (cm)
ε electrode length normalized w.r.t. the static bed length
η local overpotential (volts)
λ characteristic length (cm)
ρ solution-particle density difference (g cm^{-3})
ρ_m effective specific resistivity of the discontinuous metal phase (Ω cm)
ρ_s effective specific resistivity of the solution phase (Ω cm)
ϕ_m metal potential (volts)
ϕ_s solution potential (volts)